Urea electro-oxidation byproducts impact on NiO/NiOOH anode performance studied by operando electrochemical impedance spectroscopy

Sophia Akkari, Vincent Vivier, Carlos M Sánchez-Sánchez

Urea electro-oxidation byproducts impact on NiO/NiOOH anode performance studied by operando electrochemical impedance spectroscopy

Sophia Akkari[a], Vincent Vivier[b,*], Carlos M. Sánchez-Sánchez[a,**]

[a] Sorbonne Université, CNRS, Laboratoire Interfaces et Systèmes Electrochimiques (LISE), 4 place Jussieu, F-75005 Paris, France

[b] Sorbonne Université, CNRS, Laboratoire de Réactivité de Surface, LRS UMR 7197, F-75005 Paris, France

Corresponding author:

*e-mail: vincent.vivier@sorbonne-universite.fr (Dr. Vincent Vivier)

**e-mail: carlos.sanchez@sorbonne-universite.fr (Dr. Carlos M. Sánchez-Sánchez)

Abstract

With significant quantities of urea ($CO(NH_2)_2$) being worldwide produced and its presence at high concentration in urine, simultaneous treatment of urea effluents and hydrogen production by paired electrolysis represents a very attractive approach in circular economy. Urea electro-oxidation on Ni-based catalysts in alkaline solution represents a promising approach, but poor stability of the Ni-based catalytic performance has been reported. In this work, the performance and stability of a nanostructured NiO/NiOOH anode for urea electro-oxidation has been evaluated by electrochemical impedance spectroscopy (EIS), cyclic voltammetry (CV) and chronoamperometry (CA). Firstly, the thickness of the NiOOH active film formed during the electrochemical activation process on NiO NPs (< 50 nm) is estimated from EIS data at about 4 nm. Secondly, the impact on the catalyst performance of all previously identified urea electro-oxidation by-products (ammonia (NH_3), carbonate (CO_3^{2-}), cyanate (^-OCN) and nitrite (NO_2^-)) has been individually addressed by operando EIS, and none of them are responsible for the NiO/NiOOH catalytic deactivation. In addition to this, more insight into the competitive adsorption of $CO(NH_2)_2$ and OH^- on the catalyst surface during electrode aging was gained by the response of EIS in different potential regions.

Keywords: Urea electro-oxidation; NiOOH film thickness; Anode deactivation; Electrochemical Impedance Spectroscopy; Reaction by-products

Introduction

Urea ($CO(NH_2)_2$) is a prevalent component in wastewater effluents and its biological degradation into ammonia (NH_3) [1] can be hazardous to the environment such as causing eutrophication. Human urine contains an average of 0.33 M of urea [2], and it is estimated that an adult produces 1.5 liters of urine per day [3]. This results in the daily production of around 11.8 billion liters of urine globally, given the world's population of 7.9 billion people. Urea is also one of the most widely produced and used nitrogen-based fertilizers, with an estimated worldwide production of 180 million metric tons annually, according to Statista [4]. Thus, urea containing effluents represent an environmental issue, where effective removal of urea needs to be ensured for safety water discharge into the environment, as well as an opportunity for enabling circular economy, as urea electrolysis represents a suitable approach for hydrogen production. In recent decades, special attention has been paid to urea electrolysis [2,5–9] as an attractive paired electrolysis for simultaneous wastewater treatment and hydrogen production, where both reactions at the anode and the cathode provide valuable products. Thus, urea is electrochemically oxidized in alkaline medium at the anode into innocuous compounds such as CO_3^{2-} and N_2 (Equation 1); meanwhile hydrogen gas (H_2) is produced at the cathode from H_2O reduction (Equation 2) displaying an overall cell potential +0.02 V, which is significantly lower than H_2 production from H_2O electrolysis (-1.23 V). However, the sluggish kinetics of urea electro-oxidation causes the appearance of high overpotentials, due to the formation of NiOOH from NiO oxidation (Equation 3) as a prerequisite for achieving urea oxidation (Equation 4).

$$CO(NH_2)_2 + 8OH^- \rightarrow N_2 + CO_3^{2-} + 6H_2O + 6e^- \quad (1) \quad E° = -0.85 \text{ V } vs. \text{ SHE}$$

$$2H_2O + 2e^- \rightarrow H_2 + 2OH^- \quad (2) \quad E° = -0.83 \text{ V } vs. \text{ SHE}$$

$$NiO + OH^- \rightarrow NiOOH + e^- \quad (3) \quad E°= 0.49\ V\ vs.\ SHE$$

$$NiOOH + CO(NH_2)_2 \rightarrow Ni(OH)_2 + products \quad (4)$$

$$CO(NH_2)_2 + 8\ OH^- \rightarrow {}^-OCN + 6\ H_2O + NO_2^- + 6\ e^- \quad (5) \quad E°= -0.43\ V\ vs.\ SHE$$

NiOOH is one of the few electrocatalytic materials able to efficiently oxidize urea and for this reason, Ni-based catalysts have gained extensive attention as suitable anode for urea electro-oxidation in alkaline media [2,6,10–12]. In particular, two possible reaction pathways for urea electro-oxidation are proposed in the literature involving the interconversion of $NiO/Ni(OH)_2$ and NiOOH species [12–16]. In both cases, the same initial electrochemical step converts by oxidation the inactive $NiO/Ni(OH)_2$ anode into the active NiOOH at the surface (Equation 3). Then, either the direct electro-oxidation pathway in which urea is oxidized without reducing NiOOH (Equation 1) or the indirect electro-oxidation pathway that mediates the chemical oxidation reaction of urea (Equation 4) can take place. In the latter case, the catalytically active NiOOH is chemically reduced to the inactive $Ni(OH)_2$ by urea and is regenerated afterwards at the applied potential, which allows further oxidation of urea molecules on NiOOH. In both cases, the onset potential for urea electro-oxidation is directly controlled by the onset potential to form the active NiOOH (Equation 3). However, NiOOH anode exhibits significant and progressive catalytic deactivation during urea electro-oxidation [11,17], leading to the use of doping metals such as Co or Rh as alternative to improve the NiOOH anode performances [9,18,19]. Notably, the deactivation was attributed to the adsorption of reaction intermediates or by-products formed during urea electro-oxidation. Most of the mechanistic studies reported so far has only considered CO_2 or CO_3^{2-} as potential urea electro-oxidation by-products formed on NiOOH anodes, which could compete with urea for the active sites and then, be responsible of the

deactivation process observed [11,20]. Nevertheless, a significant amount of NH_3, cyanate (^-OCN) and nitrite (NO_2^-) ions produced from urea electrolysis has been already reported as by-products by Hopsort et al. [21]. Moreover, an alternative reaction pathway based on products detection from urea electrolysis has been recently proposed in the literature [22], which considers the formation of two different N-species during urea electro-oxidation: ^-OCN and NO_2^- ions (Equation 5). Thus, other N compounds different than N_2 were also detected during the urea electrolysis and their mechanistic impact remains unknown and needs to be evaluated. In particular, CO_3^{2-}, NH_3, ^-OCN and NO_2^- by-products [21–25] are evaluated in the present work. Consequently, identifying the deactivation source of the anode will help design the next generation of more efficient electrocatalysts for urea electrolysis.

Different Ni-based materials have been already introduced in the literature as precursor for electrogenerating active NiOOH anodes [26]. However, nanostructured NiO, which presents much higher stability in strong alkaline media than metallic Ni^0 [27], has not been deeply studied so far. In this work, we aim to study the performance and stability of the nanostructured NiO/NiOOH anode for urea electro-oxidation by cyclic voltammetry (CV) and electrochemical impedance spectroscopy (EIS) using the rotating disk electrode (RDE) [28] for controlling the hydrodynamic behavior, including at the diffusion layer. In particular, the main goal of this research is to evaluate the impact on the catalyst performance of all identified by-products formed during urea electro-oxidation (CO_3^{2-}, NH_3, NO_2^- and ^-OCN). For this purpose, EIS is applied in two different potential regions, each corresponding to different phenomena taking place on the electrode surface: On the one hand, EIS in operando conditions, which involves a potential region where the faradaic urea electro-oxidation reaction takes place. This allows to

study the by-products adsorption on the catalyst surface and the reaction mechanism by EIS, owing to its remarkable sensitivity for detecting surface modifications [29]. On the other hand, in a potential region where only purely capacitive processes are involved, which corresponds to a blocking electrode behavior [30], thus allowing to characterize the electrode aging.

Experimental section

Reagents

Chemicals purchased from Sigma Aldrich: NiO nanoparticles (diameter < 50 nm) 99.8%, Sodium Cyanate (NaOCN) 96%, Sodium Nitrite ($NaNO_2$)> 97%, Sodium carbonate (Na_2CO_3) 99.5%, Nafion™ perfluorinated resin solution (5 wt. %) and Urea ($CO(NH_2)_2$) 99.5 %. The chemicals provided from VWR Prolabo were Sodium Hydroxide (NaOH) Pellets >98 %, Ammonium sulfate ($(NH_4)_2SO_4$) 99.5 % and Isopropanol anhydrous 99.5%. Ultrapure water with resistivity >18.2 MΩ cm at 25 °C (Elga Purelab Flex, Veolia Water Technologies). All the experiments were performed at room temperature and the solution was saturated with Argon before each experiment.

NiO catalytic ink preparation

The catalytic ink was prepared to be drop-casted on the surface of a Glassy Carbon (GC) disk electrode (from PINE, diameter = 5 mm), which was previously polished with Alumina (0.05 µm) for 3 minutes and sonicated in ultrapure water (18.2 MΩ cm) in order to remove the remaining alumina from the surface of the electrode. The NiO catalytic ink was prepared by sonicating 9 mg of NiO nanoparticles (NPs) (diameter < 50 nm) in 1 mL of isopropanol for 20 minutes to ensure good dispersion. Then, 7 µL of Nafion™ perfluorinated resin solution (5 wt. %) were added to the mixture both to improve the dispersion and as a binder [31–33] Then, the mixture

was re-sonicated for an additional 15 minute period and 4 µL were drop-casted onto the polished GC disk electrode and dried at open atmosphere. The morphology and crystalline structure of NiO NPs in the catalytic ink were analyzed by Scanning Electron Microscopy (SEM) and X-Ray Diffraction (XRD) and presented in Figures S1 and S2, respectively.

Electrochemical characterization

Cyclic voltammetry (CV), chronoamperometry (CA) and electrochemical impedance spectroscopy (EIS) were performed using an electrochemical glass cell of 3 electrodes at room temperature, equipped with an electrode rotator controller (WaveVortex 10 Electrode Rotator from PINE) and a potentiostat (CHI 760E). The working electrode was prepared by drop casting 4 µL of NiO catalytic ink on a 5 mm diameter rotating disk electrode (RDE) made of GC. A graphite rod (d = 0.64 cm) was used as a counter electrode to avoid any metallic contamination in solution, and a Hg/HgO directly immersed in solution was used as a reference electrode, since it is the most stable reference electrode in strong alkaline media. Assuming an average radius of the NiO NPs of 20 nm, the NiO density of 6.7 g cm^{-3} and taking into account the catalytic ink properties, it is estimated that about 1.6 10^{11} particles of NiO are deposited on the glassy carbon electrode, thus allowing to roughly estimate the active surface area (8 cm^2). Nevertheless, the current density was calculated by considering the geometric area of the RDE (0.196 cm^2). The ratio between the electroactive surface and the geometrical area is 40. The electro-oxidation of urea at different concentrations (from 0.01 to 0.33 M) was studied in 100 mL of either 1 M or 5 M NaOH solution, previously saturated with Argon gas. CVs and CAs were performed under static (0 rpm) or rotating conditions (from 100 to 2000 rpm). All EIS measurements were performed within a frequency range of 100 kHz - 10 mHz, using a sinewave perturbation of 10

mV_{rms}, 12 points per decade and rotating the working electrode at 800 rpm. EIS experiments were collected at different potentials (0.2, 0.33, 0.43 or 0.53) V *vs*. Hg/HgO.

NiO/NiOOH anode electrochemical activation

The NiO/NiOOH anode was electrochemically activated before studying urea electro-oxidation by cycling the potential between 0.03 V to 0.77 V *vs.* Hg/HgO in 5 M NaOH at 10 mV s^{-1} for 20 consecutive cycles, as described elsewhere [17]. The result of this activation process was evaluated by CV between 0.03 and 0.6 V *vs*. Hg/HgO in 5 M NaOH. As a result of this process, the initial NiO surface became enriched with an external shell of $Ni(OH)_2$/NiOOH [26,34,35].

Results and discussions

NiO NPs are very stable in strong alkaline solution, but require an initial electrochemical activation step by potential cycling for displaying urea electro-oxidation activity. Figure 1a shows the cyclic voltammograms (CVs) of NiO NPs in the urea electro-oxidation range (from 0.03 to 0.6 V *vs.* Hg/HgO) after 0, 1, 5, 10, 15, and 20 cycles of activation. Initially, the peak current on the anodic and cathodic peaks associated with the formation of Ni(III) (0.48 V *vs.* Hg/HgO in Figure 1) and Ni(II) (0.35 V *vs.* Hg/HgO in Figure 1) species rapidly increase during the early cycles. However, this increase gradually slows down as the activation cycling continues. As a result, a stable and reproducible CV is reached after 20 activation cycles (blue line in Figures 1a and 1b) in agreement with the literature [17]. This activation process forms an external porous layer of $Ni(OH)_2$/NiOOH on NiO NPs (Figure 1b), which requires reaching oxygen evolution reaction (OER) potentials by cycling between 0.03 V and 0.77 V *vs.* Hg/HgO to be formed on the NiO surface

[26,34,35]. All results reported in this work were obtained on NiO NPs after 20 activation cycles noted as NiO/NiOOH NPs.

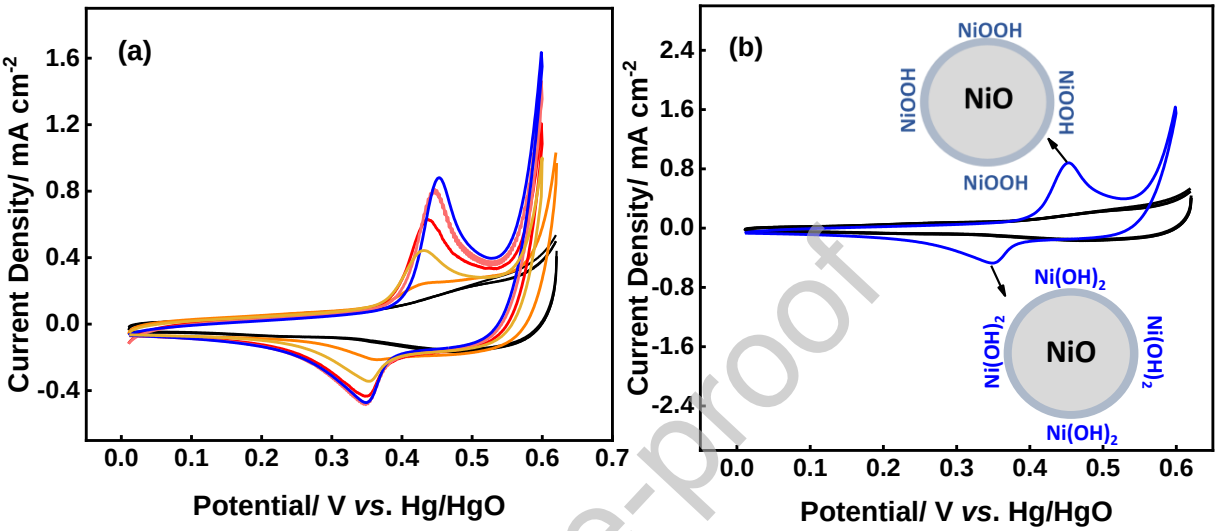

Figure 1. CV curves after the electrochemical activation of NiO NPs deposited on a RDE in 5 M NaOH solution at 800 rpm and at scan rate of 10 mV s^{-1}. (a) After activation CVs: 0 CV (black line) 1 CV (orange line), 5 CVs (yellow line), 10 CVs (red line), 15 CVs (pink line) and 20 CVs (blue line). (b) 3 consecutive CVs before activation (black line), after 20 activation CVs (blue line) and schematic representation of the $Ni(OH)_2$/NiOOH layer formed on NiO NPs.

Figure 2 shows the impact of $CO(NH_2)_2$ concentration and the combined effect of NaOH and $CO(NH_2)_2$ concentrations ([NaOH]/[$CO(NH_2)_2$]) ratio (R) on the current density obtained by electro-oxidation of urea during CAs. In particular, Figure 2 shows that the current density achieved with a solution of 0.33 M urea (R = 3) after 1600 s of electrolysis at constant potential (orange plot in Figure 2) is equivalent to that provided by a solution of 0.02 M urea, but with R = 33 (black plot in Figure 2). Moreover, increasing from 0.01 to 0.1 M the urea concentration only

provides a modest increase in current density of approx. 10-15 % (black line in Figure 2), the variation of the resultant oxidation current density for each urea concentration is clearly stated in Table S1. The relevant impact of the NaOH/$CO(NH_2)_2$ concentrations ratio has been previously investigated in the literature [36], which identified R > 8 as optimal conditions for urea electro-oxidation. Otherwise, OH^- in solution required as reactant for urea electro-oxidation (Equations 1 and 5), but also as supporting electrolyte, will not be in sufficient quantity to prevent the migration of electroactive species and ensure rapid regeneration of the OH^- species consumed in the diffusion layer at the anode (Equations 1 and 5). For this reason, R = 500 (5 M [NaOH] / 0.01 M [$CO(NH_2)_2$]) is used in the present work for studying the effect of urea electro-oxidation by-products by EIS in order to disregard any migration effect.

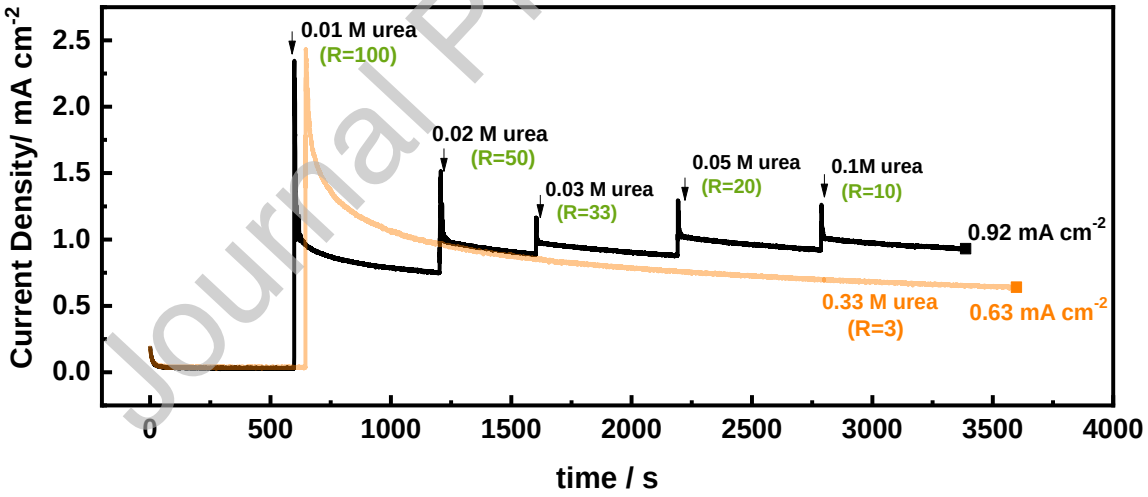

Figure 2. Chronoamperommetry curves of NiO/NiOOH NPs deposited on a RDE in 1 M NaOH at 0.45 V *vs.* Hg/HgO, different ratios [NaOH]/[$CO(NH_2)_2$] and at a rotation rate of 800 rpm. Each vertical arrow in the black plot indicates the addition of urea in the solution.

Figure 3a shows 3 consecutive potential cycles on a NiO/NiOOH electrode in the absence of urea in solution (black line) and in the presence of 0.01 M urea (blue line). NiO/NiOOH NPs in a 5 M NaOH solution exhibit good stability and the characteristic oxidation-reduction peaks for $Ni(OH)_2$/NiOOH remain unchanged along the potential cycles (black line in Figure 3a). In contrast, in the presence of 0.01 M urea (R = 500), the oxidation current is amplified due to the urea electro-oxidation reaction, but it slightly decreases after each new cycle (blue line in Figure 3a). This deactivation behavior of the catalyst is more evident at higher concentration of urea (0.33 M, R = 15). Thus, Figure 3b shows 6 consecutive potential cycles on NiO/NiOOH NPs in the presence of 0.33M urea (green and orange lines), where it is evidenced that the current density associated with urea electro-oxidation decreases after each new cycle, which has been previously attributed to the catalyst deactivation in the literature [6,13,17,20,24,37]. The different voltammetric response observed in Figures 3a and 3b as a function of urea concentration is attributed to the difference in [NaOH]/[$CO(NH_2)_2$] ratio, a more detailed study is included in Figure S3.

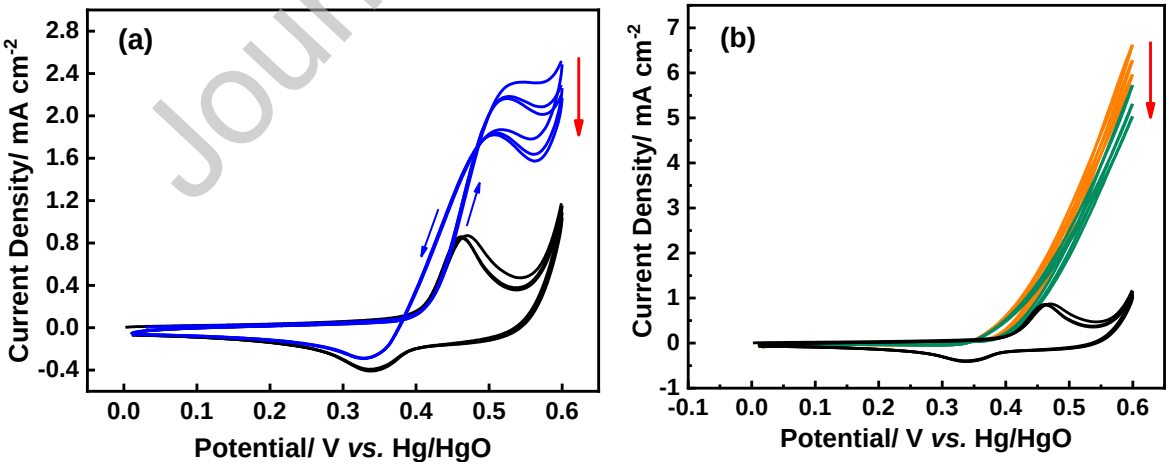

Figure 3. CVs of NiO/NiOOH NPs deposited on a RDE at rotation rate of 800 rpm and scan rate 10 mV s^{-1}. (a) 5 M NaOH (black line) and 0.01 M urea (blue line) and (b) 5 M NaOH (black line) and 0.33 M urea (orange line: cycle 1-3 and green line: cycle 4-6). Red arrows show the start and the end of the consecutive cycles.

Figure 4 presents the CA curve, which shows the current density evolution as a function of time for NiO/NiOOH NPs in a solution containing 1 M NaOH and 0.33 M urea (R = 3) at 0.53 V *vs.* Hg/HgO, along with the influence of varying electrode rotation rate. At this potential (0.53 V *vs.* Hg/HgO), the urea electro-oxidation reaction is under mass-transfer control conditions. Thus, it is typically expected that higher rotation rates would lead to an increase in the current density from urea electro-oxidation associated with a decrease in the thickness of the diffusion layer. However, the i-t curve presented in Figure 4 shows that the current density only increases when the rotation rate of the electrode increases from 0 to 400 rpm, but then gradually decreases over time regardless of the increase in the electrode rotation rate. This behavior showing mass-transfer control of urea electro-oxidation only at low rotation speeds is in agreement with the literature [11] and shows that the urea electro-oxidation reaction is mainly limited by kinetics. Moreover, the continuous decline in current density displayed in Figure 4 from 2.5 mA cm^{-2} at 200 s to 1.6 mA cm^{-2} at 1200 s clearly demonstrates a fast catalyst deactivation at 0.53 V *vs.* Hg/HgO. But it also demonstrates higher activity for urea electro-oxidation at this applied potential than at 0.45 V *vs.* Hg/HgO, as shown in Figure 2 (orange plot, 0.96 mA cm^{-2} at 1200 s).

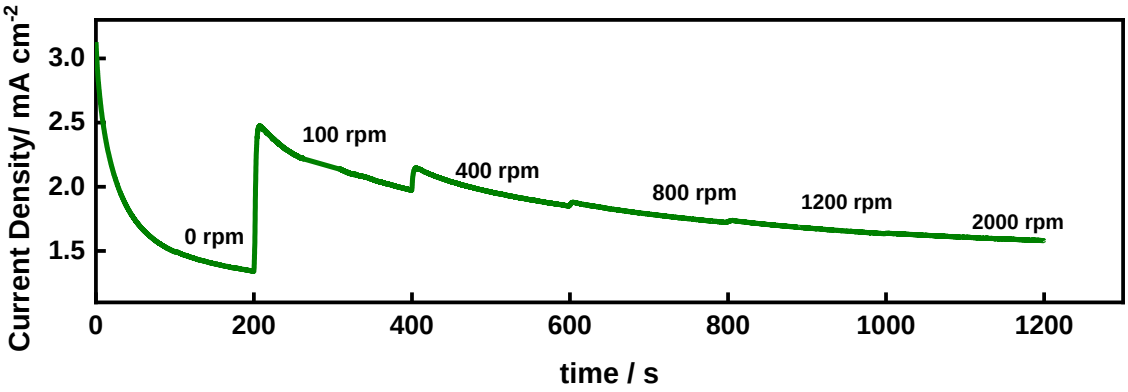

Figure 4. Chronoamperommetry curve of NiO/NiOOH NPs deposited on a RDE in 1 M NaOH and 0.33 M urea at 0.53V *vs.* Hg/HgO and different electrode rotation rates.

Figure 5 displays the Nyquist plots corresponding to EIS spectra obtained on the NiO/NiOOH NPs electrode in both presence and absence of urea in solution at different polarization potentials. Figures 5a and 5b show the EIS responses at 0.33 V, 0.43 V and 0.53 V *vs*. Hg/HgO in a Nyquist representation, in the absence of urea in solution. At 0.33 V *vs*. Hg/HgO (green plots in Figures 5a and 5b), a capacitive behavior is observed in the high frequency domain, which corresponds to the interfacial capacitance (electric double layer and the contribution of the oxide film formed at the NP surface), which is in agreement with CV results reported in Figure 3a (black line). In contrast, at 0.43 V and 0.53 V *vs*. Hg/HgO (grey and orange plots, respectively in Figures 5a and 5b), a semicircle loop with a characteristic frequency of 146 Hz is clearly observed in the Nyquist plot zoomed at high frequency (Figure 5b). This is attributed to the charge-transfer process associated to the $NiO/Ni(OH)_2$ oxidation into NiOOH at the electrode surface. In addition to this, at 0.53 V *vs*. Hg/HgO (orange plots in Figures 5a and 5b), an additional time-constant is observed with a characteristic frequency of 0.04 Hz, which may be attributed to the relaxation of the adsorbed OH^-. The Nyquist plots in Figures 5c and 5d show the impact of different polarization

potentials applied in the presence of urea in solution. Figure 5d, which zooms the high frequency domain of Figure 5c shows no difference in comparison with Figure 5b. This demonstrates that the capacitive behavior observed at 0.33 V *vs*. Hg/HgO (green plot) and the charge-transfer process (characteristic frequency of 146 Hz) associated with the $NiO/Ni(OH)_2$ oxidation into NiOOH at the electrode surface, are not affected by the presence of urea in solution. In contrast, at 0.43 V *vs*. Hg/HgO, an additional time-constant appears with a characteristic frequency of 0.46 Hz (grey plot in Figure 5c), which may be attributed to the urea electro-oxidation in agreement with CV results reported in Figure 3a (blue plot). At 0.53 V *vs*. Hg/HgO, during urea electro-oxidation as well, but under mass-transfer control, a reverse semicircle loop is observed in the Nyquist plot (blue plot in Figure 5c), which represents a negative polarization resistance (R_p <0). As noted in literature [38,39], a negative value of polarization resistance is obtained by EIS when the applied potential is located in the negative slope region of the current-potential curve (Figure 3a, blue line), indicating that the measurement has been performed on an operating point of the current-voltage curve with a negative slope. This negative R_p value results in a reverse capacitive loop, regardless of either the presence or absence of any adsorption process, which sometimes has been confusedly attributed to adsorption on the electrode surface in previous EIS studies regarding urea electro-oxidation [6,13]. Nevertheless, the EIS data in the low frequency domain at 0.53 V *vs*. Hg/HgO in the presence of urea show a new time constant with a characteristic frequency of 0.15 Hz (blue plot in Figure 5c). Thus, Figure 5e corresponds to a new Nyquist plot only comparing the EIS data at 0.53 V *vs*. Hg/HgO in the absence (orange plot) and the presence (blue plot) of urea and Figure 5f corresponds to a zoom in the high frequency domain of Figure 5e. As previously

mentioned, the process at 146 Hz shown in Figure 5f remains constant, as well as that at 0.04 Hz (Figure 5e) associated to the relaxation of the adsorbed OH^-. In contrast, when urea is present in solution (blue plot in Figure 5e), an additional time constant appears at 0.15 Hz, which is associated to a relaxation of an adsorbed species from either the products/by-products generated during the electro-oxidation of urea or by the adsorption of urea itself on the surface of the electrode. Tables 1 and 2 summarize the characteristic parameters extracted by graphical analysis from EIS measurements shown in Figure 5. F is the frequency, R_e, R_{ct}, and R_p are the electrolyte, charge transfer and polarization resistance, respectively. Z_i is the imaginary part of impedance. C_{LF} and C_{int} are the low frequency (LF) and interfacial capacitance, respectively.

Table 1. EIS parameters of NiO NPs in 5 M NaOH solution.

Potential/ V *vs.* Hg/HgO	**F (Hz)**	**R_e (Ω cm^2)**	**R_{ct} (Ω cm^2)**	**Z_i (Ω cm^2)**	**C_{LF} (µF cm $^{-2}$)**	**C_{int} (µF cm $^{-2}$)**
0.33	0.02	1.4 ± 0.1	-	6646.1 ± 0.1	1.1 ± 0.1	-
0.53	146	0.9 ± 0.1	8.6 ± 0.1	-	-	0.12 ± 0.01

Table 2. EIS parameters of NiO NPs in 5 M NaOH and 0.01 M urea solution.

Potential/ V *vs.* Hg/HgO	**F (Hz)**	**R_e (Ω cm^2)**	**R_{ct} (Ω cm^2)**	**R_p (Ω cm^2)**	**C_{LF} (µF cm $^{-2}$)**	**C_{int} (µF cm $^{-2}$)**
0.33	0.4	1.4 ± 0.1	-	-	-	-
0.53	146	1.5 ± 0.1	8.7± 0.1	-	-	0.12 ± 0.01
0.53	0.15	1.5 ± 0.1	-	-140.7 ± 0.1	-	-

The charge-transfer process associated with the $NiO/Ni(OH)_2$ oxidation into NiOOH at the electrode surface (characteristic frequency of 146 Hz) observed at 0.53 V *vs*. Hg/HgO (Figure 5f) allows to estimate the thickness of the formed NiOOH film from the EIS data. As far as we know, the thickness of the NiOOH layer generated through electrochemical activation and shown in Figure 1 has not been estimated before in the literature. The resulting high frequency capacitance (C_∞) obtained from EIS data by Cole-Cole plot is 0.5 µF (in the range of 2.5 µF cm^{-2}). Assuming a permittivity (ε) of 12 for the NiO/NiOOH layer and neglecting the double layer capacitance (which should be one order of magnitude larger), the thickness of the oxide layer (*d*) formed at the electrode surface can be easily calculated from Equation 6 [40] where ε_0 corresponds to the vacuum permittivity. The NiOOH active film formed during the electrochemical activation process on NiO NPs is estimated at about 4 nm. Interestingly, this value is in agreement with the NiO particle dimension (diameter < 50 nm).

$$C_\infty = \frac{\varepsilon \varepsilon_0}{d} \qquad (6)$$

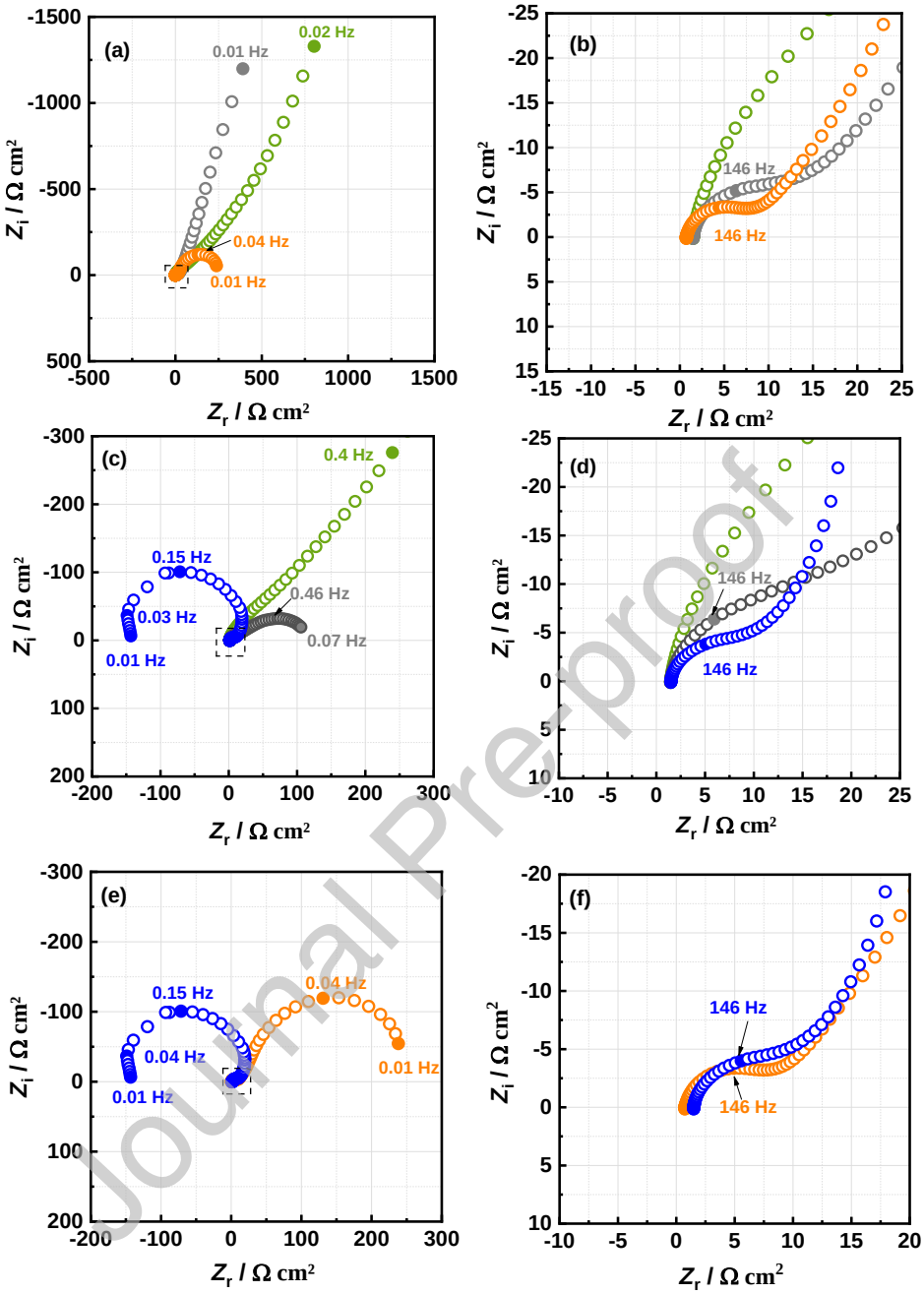

Figure 5. Nyquist plots corresponding to EIS spectra obtained on NiO/NiOOH NPs at 800 rpm in 5 M NaOH solution. (a) at different polarization potentials 0.33 V *vs.* Hg/HgO (green), 0.43 V *vs.* Hg/HgO (grey), and 0.53 V *vs.* Hg/HgO (orange), (b) Figure 5a zoomed in the high frequency domain, (c) in the presence of 0.01 M urea in solution at different polarization potentials 0.33 V *vs.* Hg/HgO (green), 0.43 V *vs.* Hg/HgO (grey) and 0.53 V *vs.* Hg/HgO (blue), (d) Figure 5c zoomed

in the high frequency domain, (e) at 0.53 V *vs.* Hg/HgO in the absence (orange plot) and the presence (blue plot) of 0.01 M urea in solution and (f) Figure 5e zoomed in the high frequency domain.

To investigate the effect of urea and urea electro-oxidation by-products (CO_3^{2-}, NH_3, ^-OCN and NO_2^-) on the NiO/NiOOH catalyst's surface, EIS diagrams were collected and compared in absence and in presence of each single by-product. Figure 6 shows the corresponding EIS diagrams normalized by the low frequency value of the real part of the impedance in order to provide the easiest comparison and to avoid any effect of the active surface area. Those EIS measurements were performed at 0.53 V *vs.* Hg/HgO to specifically enhance the deactivation process of the catalyst during urea electro-oxidation. Moreover, solutions containing low urea concentration and high $NaOH/CO(NH_2)_2$ ratio are used for minimizing the competition for the active sites of the electrocatalyst between urea and urea electro-oxidation by-products. The results shown in Figure 6a indicate that the electrochemical response of NiO/NiOOH NPs in 5 M NaOH (black plot) is not sensitive to the presence of CO_3^{2-} (red plot), NO_2^-(blue plot), ^-OCN (green plot) or NH_3 (orange plot). Likewise, no significant effect of those same compounds is neither observed in the presence of urea (Figure 6b), which demonstrates that none of these products (CO_3^{2-}, NO_2^-, ^-OCN, and NH_3) is responsible for the NiO/NiOOH NP surface deactivation shown in Figure 4. Moreover, these EIS results have also demonstrated that the appearance of a reverse loop phenomena (Figure 6b) is not an evidence of urea electro-oxidation byproduct adsorption, but is only linked to the current decrease with increasing potential [38,39]. However, urea adsorption cannot be ruled out as a cause of electrode deactivation.

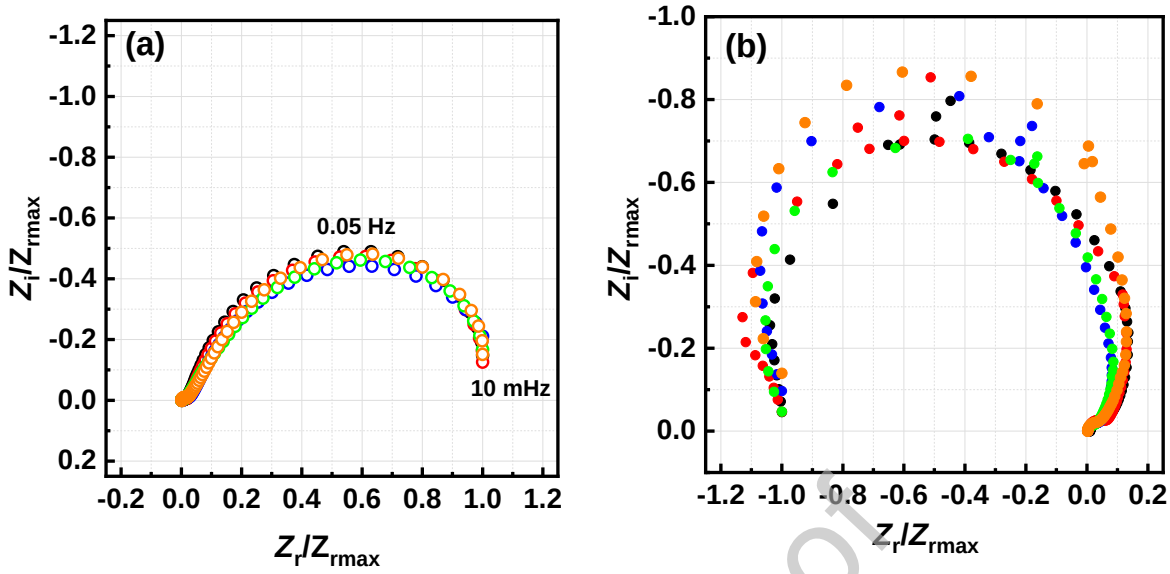

Figure 6. Normalized Nyquist plots corresponding to EIS spectra obtained on NiO/NiOOH NPs at 800 rpm and 0.53 V *vs.* Hg/HgO. Solution composition: (a) 5 M NaOH (black plot) and (b) 5 M NaOH and 0.01 M urea (black plot). In presence of 0.01 M CO_3^{2-} (red plot), 0.01 M NO_2^- (blue plot), 0.01 M ^-OCN (green plot), or 0.01 M NH_3 (orange plot) in solution.

Figure 7 shows the Nyquist plots corresponding to EIS spectra obtained on the NiO/NiOOH NPs electrode at 0.2 V *vs.* Hg/HgO, a potential region where only purely capacitive processes are involved. Those EIS data allow to evaluate the electrode aging and any surface modification resulted from being exposed to urea. To investigate this, the electrode is examined by EIS before and after undergoing immersion in urea solution and urea electro-oxidation either by CV or electrolysis. Figure 7a compares the Nyquist plots of the electrode immersed in a urea-free solution (black plot), immersed 1 h in a 0.33 M urea solution (green plot) and after performing 1 CV cycle up to 0.6 V *vs*. Hg/HgO in a 0.33 M urea solution (red plot). All these EIS results are almost identical. Additionally, Figure 7b shows that the electrode surface is not modified after 1 hour of electrolysis at 0.53 V *vs.* Hg/HgO in a 0.33 M urea solution (orange plot). This suggests

that none of the byproducts generated during urea electro-oxidation remains adsorbed on the electrode's surface. Moreover, Figure 7 also suggests that the deactivation of NiO/NiOOH NPs shown in Figure 4 by a significant decrease in current density at 0.53 V *vs.* Hg/HgO is most likely not due to the adsorption of urea. However, it is demonstrated that urea competes with OH^- for the active sites at the electrode surface for its electro-oxidation [12,14]. The low frequency limit of the imaginary part of the impedance allow to roughly estimate the capacitive response of the electrode. To convert the response of CPE into a capacitive value, the Brug formula [41,42] is employed, resulting in an approximate capacitance of 25 µF cm^{-2}. Based on this analysis, we can conclude that in this potential domain, and at low frequencies, the determined capacitance is consistent with a double layer capacitance in line with the work of Gharbi et al. [43] who showed that the capacitive behavior of the interface can usually be analyzed in this frequency domain.

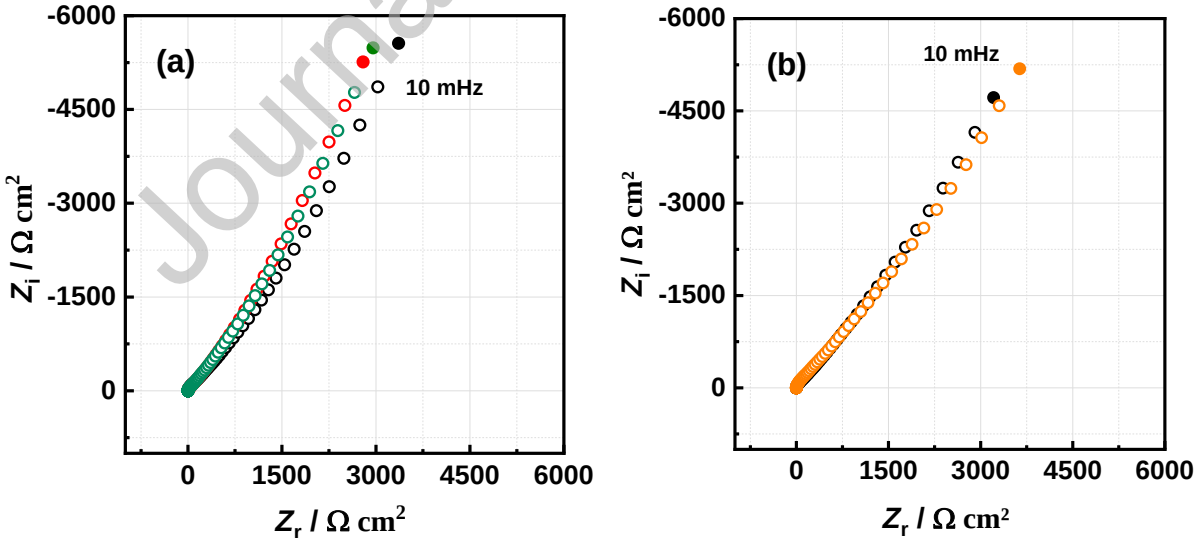

Figure 7. Nyquist plots corresponding to EIS spectra obtained on NiO/NiOOH NPs at 800 rpm and 0.2 V *vs.* Hg/HgO in 5 M NaOH solution (black plots). (a) After performing a CV cycle up to 0.6 V

vs. Hg/HgO (scan rate 10 mV s^{-1}) in 5 M NaOH and 0.33 M urea solution (red plot), and after electrode immersion for 1 h in 5 M NaOH and 0.33 M urea solution (green plot). (b) After 1 h of electrolysis at 0.53 V *vs.* Hg/HgO in 5 M NaOH and 0.33 M urea solution (orange plot).

Conclusions

NiO NPs enriched by electrochemical activation with an external shell of $Ni(OH)_2$/NiOOH exhibit high stability in strong alkaline solution, but very few examples of application into the urea electro-oxidation has been reported so far. This study evaluates the performance and stability of a nanostructured NiO/NiOOH anode for urea electro-oxidation using various electrochemical techniques. Cyclic voltammetry and chronoamperommetry analysis strongly suggest the occurrence of a catalyst deactivation process during urea electro-oxidation. EIS data reported here demonstrate that the charge-transfer process associated to the NiO/$Ni(OH)_2$ oxidation into NiOOH at the electrode surface is insensitive to the presence of urea in solution. This allows to estimate the thickness of the NiOOH active film on the NiO NPs (4 nm) by EIS. In addition to that, EIS data show the presence of two time-constants in the low-frequency domain, which are attributed to the relaxation of the adsorbed OH^- and urea. The operando EIS results performed at 0.53 V *vs.* Hg/HgO, indicated that urea electro-oxidation by-products (CO_3^{2-}, ^-OCN, NH_3 and NO_2^-) do not have substantial impact on the catalytic activity of the NiO/NiOOH anode. Furthermore, EIS data at 0.2 V *vs.* Hg/HgO, where only purely capacitive processes are involved, demonstrate neither urea adsorption impact on catalyst deactivation nor notable aging effects during the first hour of urea electro-oxidation. In conclusion, this work is showing a significant limitation for the NiO/NiOOH anodes application in urea treatment due to the catalyst

deactivation and has ruled out the responsibility on this from urea and urea electro-oxidation byproduct (CO_3^{2-}, ^-OCN, NH_3 and NO_2^-) adsorption. Thus, we suggest to address in future studies the ability of NiO to regenerate the NiOOH active film as a way to understand the catalyst deactivation issue, which should contribute to find more efficient and sustainable urea treatment technologies.

Acknowledgements

The authors acknowledge the support of the Centre National de la Recherche Scientifique (CNRS) and the funding from the ANR (ANR-19-CE04-0009-02) project HYUREA.

CRediT authorship contribution statement

Sophia Akkari: Formal analysis, Investigation, Methodology, Validation, Visualization, Writing – original draft. **Vincent Vivier**: Conceptualization, Formal analysis, Funding acquisition, Investigation, Supervision, Validation, Writing – review & editing. **Carlos M. Sánchez-Sánchez**: Conceptualization, Formal analysis, Funding acquisition, Investigation, Methodology, Project administration, Supervision, Validation, Writing – review & editing.

Supplementary materials

Supplementary material associated with this article can be found in the online version.

References

[1] J.J. Sigurdarson, S. Svane, H. Karring, The molecular processes of urea hydrolysis in relation to ammonia emissions from agriculture, Rev Environ Sci Biotechnol. 17 (2018) 241–258. https://doi.org/10.1007/s11157-018-9466-1.

[2] B.K. Boggs, R.L. King, G.G. Botte, Urea electrolysis: direct hydrogen production from urine, Chem. Commun. (2009) 4859–4861. https://doi.org/10.1039/B905974A.

[3] W. Rauch, D. Brockmann, I. Peters, T.A. Larsen, W. Gujer, Combining urine separation with waste design: an analysis using a stochastic model for urine production, Water Research. 37 (2003) 681–689. https://doi.org/10.1016/S0043-1354(02)00364-0.

[4] International Fertilizer Industry Association, Urea production worldwide, Statista. (2021). https://www.statista.com/statistics/1287028/global-urea-production/ (accessed April 19, 2023).

[5] K. Ye, G. Wang, D. Cao, G. Wang, Recent Advances in the Electro-Oxidation of Urea for Direct Urea Fuel Cell and Urea Electrolysis, Top Curr Chem (Z). 376 (2018) 42. https://doi.org/10.1007/s41061-018-0219-y.

[6] F. Guo, K. Ye, K. Cheng, G. Wang, D. Cao, Preparation of nickel nanowire arrays electrode for urea electro-oxidation in alkaline medium, Journal of Power Sources. 278 (2015) 562–568. https://doi.org/10.1016/j.jpowsour.2014.12.125.

[7] W. Xu, Z. Wu, S. Tao, Urea-Based Fuel Cells and Electrocatalysts for Urea Oxidation, Energy Technology. 4 (2016) 1329–1337. https://doi.org/10.1002/ente.201600185.

[8] R. Lan, S. Tao, J.T.S. Irvine, A direct urea fuel cell – power from fertiliser and waste, Energy Environ. Sci. 3 (2010) 438–441. https://doi.org/10.1039/B924786F.

[9] P. Mirzaei, S. Bastide, A. Dassy, R. Bensimon, J. Bourgon, A. Aghajani, C. Zlotea, D. Muller-Bouvet, C. Cachet-Vivier, Electrochemical oxidation of urea on nickel-rhodium nanoparticles/carbon composites, Electrochimica Acta. 297 (2019) 715–724. https://doi.org/10.1016/j.electacta.2018.11.205.

[10] W. Yan, D. Wang, L.A. Diaz, G.G. Botte, Nickel nanowires as effective catalysts for urea electro-oxidation, Electrochimica Acta. 134 (2014) 266–271. https://doi.org/10.1016/j.electacta.2014.03.134.

[11] V. Vedharathinam, G.G. Botte, Understanding the electro-catalytic oxidation mechanism of urea on nickel electrodes in alkaline medium, Electrochimica Acta. 81 (2012) 292–300. https://doi.org/10.1016/j.electacta.2012.07.007.

[12] V. Vedharathinam, G.G. Botte, Direct evidence of the mechanism for the electro-oxidation of urea on Ni(OH)2 catalyst in alkaline medium, Electrochimica Acta. 108 (2013) 660–665. https://doi.org/10.1016/j.electacta.2013.06.137.

[13] F. Guo, K. Ye, M. Du, X. Huang, K. Cheng, G. Wang, D. Cao, Electrochemical impedance analysis of urea electro-oxidation mechanism on nickel catalyst in alkaline medium, Electrochimica Acta. 210 (2016) 474–482. https://doi.org/10.1016/j.electacta.2016.05.149.

[14] D.A. Daramola, D. Singh, G.G. Botte, Dissociation rates of urea in the presence of NiOOH catalyst: a DFT analysis, J Phys Chem A. 114 (2010) 11513–11521. https://doi.org/10.1021/jp105159t.

[15] C. Carlesi Jara, S. Di Giulio, D. Fino, P. Spinelli, Combined direct and indirect electroxidation of urea containing water, J Appl Electrochem. 38 (2008) 915–922. https://doi.org/10.1007/s10800-008-9496-4.
[16] D. Wang, G.G. Botte, In Situ X-Ray Diffraction Study of Urea Electrolysis on Nickel Catalysts, ECS Electrochem. Lett. 3 (2014) H29–H32. https://doi.org/10.1149/2.0031409eel.
[17] R.H. Tammam, M.M. Saleh, On the electrocatalytic urea oxidation on nickel oxide nanoparticles modified glassy carbon electrode, Journal of Electroanalytical Chemistry. 794 (2017) 189–196. https://doi.org/10.1016/j.jelechem.2017.04.023.
[18] M. Vidotti, M.R. Silva, R.P. Salvador, S.I.C. de Torresi, L.H. Dall'Antonia, Electrocatalytic oxidation of urea by nanostructured nickel/cobalt hydroxide electrodes, Electrochimica Acta. 53 (2008) 4030–4034. https://doi.org/10.1016/j.electacta.2007.11.029.
[19] J. Vilana, E. Gómez, E. Vallés, Influence of the composition and crystalline phase of electrodeposited CoNi films in the preparation of CoNi oxidized surfaces as electrodes for urea electro-oxidation, Applied Surface Science. 360 (2016) 816–825. https://doi.org/10.1016/j.apsusc.2015.11.072.
[20] R.P. Forslund, J.T. Mefford, W.G. Hardin, C.T. Alexander, K.P. Johnston, K.J. Stevenson, Nanostructured LaNiO3 Perovskite Electrocatalyst for Enhanced Urea Oxidation, ACS Catal. 6 (2016) 5044–5051. https://doi.org/10.1021/acscatal.6b00487.
[21] G. Hopsort, D.P.D. Carmo, L. Latapie, K. Loubière, K.G. Serrano, T. Tzedakis, Progress toward a better understanding of the urea oxidation by electromediation of Ni(III)/Ni(II) system in alkaline media, Electrochimica Acta. 442 (2023) 141898. https://doi.org/10.1016/j.electacta.2023.141898.
[22] S.W. Tatarchuk, J.J. Medvedev, F. Li, Y. Tobolovskaya, A. Klinkova, Nickel-Catalyzed Urea Electrolysis: From Nitrite and Cyanate as Major Products to Nitrogen Evolution, Angewandte Chemie International Edition. 61 (2022) e202209839. https://doi.org/10.1002/anie.202209839.
[23] J. Li, J. Li, T. Liu, L. Chen, Y. Li, H. Wang, X. Chen, M. Gong, Z.-P. Liu, X. Yang, Deciphering and Suppressing Over-Oxidized Nitrogen in Nickel-Catalyzed Urea Electrolysis, Angewandte Chemie International Edition. 60 (2021) 26656–26662. https://doi.org/10.1002/anie.202107886.
[24] L. Wang, S. Zhu, N. Marinkovic, S. Kattel, M. Shao, B. Yang, J.G. Chen, Insight into the synergistic effect between nickel and tungsten carbide for catalyzing urea electrooxidation in alkaline electrolyte, Applied Catalysis B: Environmental. 232 (2018) 365–370. https://doi.org/10.1016/j.apcatb.2018.03.064.
[25] H. Qin, Y. Ye, J. Li, W. Jia, S. Zheng, X. Cao, G. Lin, L. Jiao, Synergistic Engineering of Doping and Vacancy in Ni(OH)2 to Boost Urea Electrooxidation, Advanced Functional Materials. 33 (2023) 2209698. https://doi.org/10.1002/adfm.202209698.
[26] Y. Miao, L. Ouyang, S. Zhou, L. Xu, Z. Yang, M. Xiao, R. Ouyang, Electrocatalysis and electroanalysis of nickel, its oxides, hydroxides and oxyhydroxides toward small molecules, Biosensors and Bioelectronics. 53 (2014) 428–439. https://doi.org/10.1016/j.bios.2013.10.008.
[27] L.-F. Huang, M.J. Hutchison, R.J.Jr. Santucci, J.R. Scully, J.M. Rondinelli, Improved Electrochemical Phase Diagrams from Theory and Experiment: The Ni–Water System and

Its Complex Compounds, J. Phys. Chem. C. 121 (2017) 9782–9789. https://doi.org/10.1021/acs.jpcc.7b02771.

[28] A.J. Bard, L.R. Faulkner, Electrochemical Methods. Fundamentals and Applications. , 2nd edition, 2001., n.d.

[29] S. Wang, J. Zhang, O. Gharbi, V. Vivier, M. Gao, M.E. Orazem, Electrochemical impedance spectroscopy, Nat Rev Methods Primers. 1 (2021) 1–21. https://doi.org/10.1038/s43586-021-00039-w.

[30] M. Musiani, M. Orazem, B. Tribollet, V. Vivier, Impedance of blocking electrodes having parallel cylindrical pores with distributed radii, Electrochimica Acta. 56 (2011) 8014–8022. https://doi.org/10.1016/j.electacta.2010.12.004.

[31] J. Chlistunoff, J.-M. Sansiñena, On the use of Nafion® in electrochemical studies of carbon supported oxygen reduction catalysts in aqueous media, Journal of Electroanalytical Chemistry. 780 (2016) 134–146. https://doi.org/10.1016/j.jelechem.2016.09.014.

[32] L. Zhang, J.V. Perales-Rondón, A. Thomère, J. Blanchard, C.M. Sánchez-Sánchez, Platinum-zeolite hybrid catalyst for the electrooxidation of formic acid, Journal of Electroanalytical Chemistry. 896 (2021) 115491. https://doi.org/10.1016/j.jelechem.2021.115491.

[33] R. Venegas, K. Muñoz-Becerra, S. Juillard, L. Zhang, R. Oñate, I. Ponce, V. Vivier, F.J. Recio, C.M. Sánchez-Sánchez, Proving ligand structure-reactivity correlation on multinuclear copper electrocatalysts supported on carbon black for the oxygen reduction reaction, Electrochimica Acta. 434 (2022) 141304. https://doi.org/10.1016/j.electacta.2022.141304.

[34] Q. Yi, J. Zhang, W. Huang, X. Liu, Electrocatalytic oxidation of cyclohexanol on a nickel oxyhydroxide modified nickel electrode in alkaline solutions, Catalysis Communications. 8 (2007) 1017–1022. https://doi.org/10.1016/j.catcom.2006.10.009.

[35] A.G. Oshchepkov, A. Bonnefont, V.A. Saveleva, V. Papaefthimiou, S. Zafeiratos, S.N. Pronkin, V.N. Parmon, E.R. Savinova, Exploring the Influence of the Nickel Oxide Species on the Kinetics of Hydrogen Electrode Reactions in Alkaline Media, Top Catal. 59 (2016) 1319–1331. https://doi.org/10.1007/s11244-016-0657-0.

[36] K. Ye, H. Zhang, L. Zhao, X. Huang, K. Cheng, G. Wang, D. Cao, Facile preparation of three-dimensional Ni(OH)2/Ni foam anode with low cost and its application in a direct urea fuel cell, New J. Chem. 40 (2016) 8673–8680. https://doi.org/10.1039/C6NJ01648K.

[37] Q. Zhang, F.MD. Kazim, S. Ma, K. Qu, M. Li, Y. Wang, H. Hu, W. Cai, Z. Yang, Nitrogen dopants in nickel nanoparticles embedded carbon nanotubes promote overall urea oxidation, Applied Catalysis B: Environmental. 280 (2021) 119436. https://doi.org/10.1016/j.apcatb.2020.119436.

[38] D.D. Macdonald, Review of mechanistic analysis by electrochemical impedance spectroscopy, Electrochimica Acta. 35 (1990) 1509–1525. https://doi.org/10.1016/0013-4686(90)80005-9.

[39] M. Keddam, 2006 W.R. Whitney Award Lecture: Application of Advanced Electrochemical Techniques and Concepts to Corrosion Phenomena, Corrosion. 62 (2006) 1056–1066. https://doi.org/10.5006/1.3278239.

[40] M. Benoit, C. Bataillon, B. Gwinner, F. Miserque, M.E. Orazem, C.M. Sánchez-Sánchez, B. Tribollet, V. Vivier, Comparison of different methods for measuring the passive film thickness on metals, Electrochimica Acta. 201 (2016) 340–347. https://doi.org/10.1016/j.electacta.2015.12.173.

[41] B. Hirschorn, M.E. Orazem, B. Tribollet, V. Vivier, I. Frateur, M. Musiani, Determination of effective capacitance and film thickness from constant-phase-element parameters, Electrochimica Acta. 55 (2010) 6218–6227. https://doi.org/10.1016/j.electacta.2009.10.065.
[42] S.M. Gateman, O. Gharbi, H. Gomes de Melo, K. Ngo, M. Turmine, V. Vivier, On the use of a constant phase element (CPE) in electrochemistry, Current Opinion in Electrochemistry. 36 (2022) 101133. https://doi.org/10.1016/j.coelec.2022.101133.
[43] O. Gharbi, M.T.T. Tran, M.E. Orazem, B. Tribollet, M. Turmine, V. Vivier, Impedance Response of a Thin Film on an Electrode: Deciphering the Influence of the Double Layer Capacitance, ChemPhysChem. 22 (2021) 1371–1378. https://doi.org/10.1002/cphc.202100177.

GRAPHICAL ABSTRACT

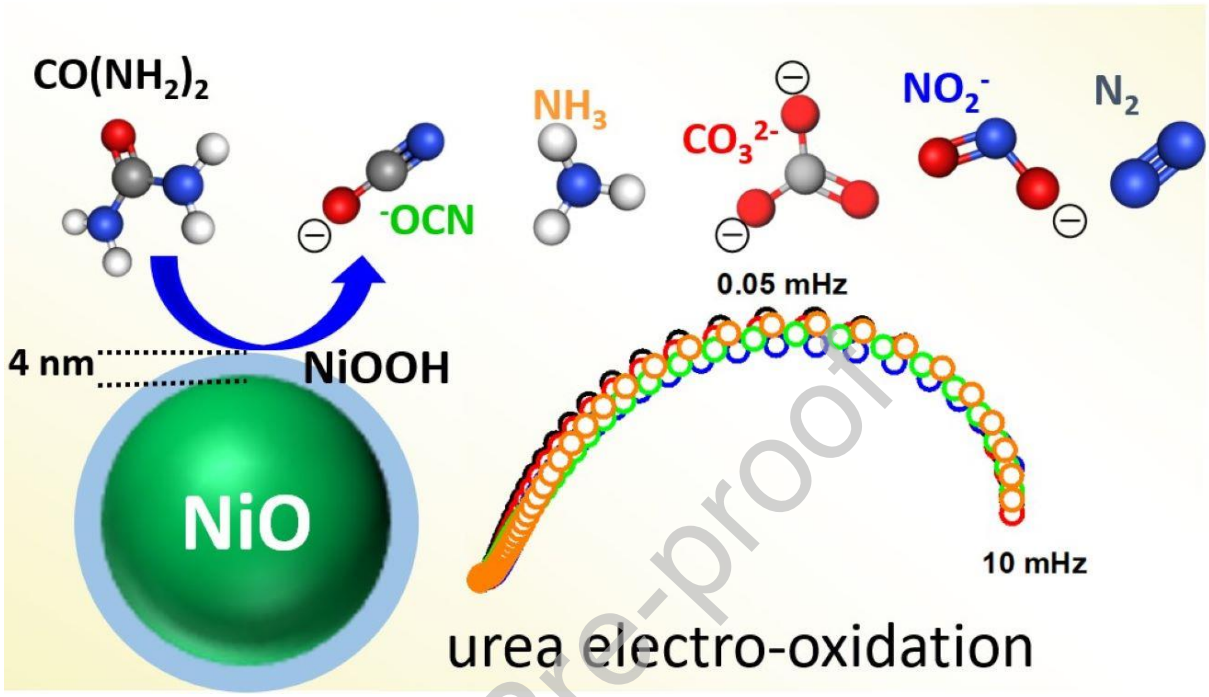

CRediT authorship contribution statement

Sophia Akkari: Formal analysis, Investigation, Methodology, Validation, Visualization, Writing – original draft. **Vincent Vivier**: Conceptualization, Formal analysis, Funding acquisition, Investigation, Supervision, Validation, Writing – review & editing. **Carlos M. Sánchez-Sánchez**: Conceptualization, Formal analysis, Funding acquisition, Investigation, Methodology, Project administration, Supervision, Validation, Writing – review & editing.

Declaration of interests

☒ The authors declare that they have no known competing financial interests or personal relationships that could have appeared to influence the work reported in this paper.

☐The authors declare the following financial interests/personal relationships which may be considered as potential competing interests: